IL NUOVO CIMENTO Vol. 35 C, N. 1 Gennaio-Febbraio 2012
DOI 10.1393/ncc/i2012-11127-7

Colloquia: LaThuile11

Heavy-ion physics with the ATLAS detector at the LHC

P. Steinberg for the ATLAS Collaboration
Brookhaven National Laboratory - Upton, NY, USA

(ricevuto il 29 Settembre 2011; pubblicato online il 23 Gennaio 2012)

Summary. — First results on jet, $J\psi$ and Z production are presented from the first lead-lead run at the LHC, using the ATLAS detector. The transverse energies of opposed dijets are observed to show greater asymmetry with increasing event centrality, something not observed in proton-proton collisions. This may point to an interpretation in terms of strong jet energy loss in a hot, dense medium. Also, using the ATLAS muon spectrometer, a centrality-dependent suppression has been observed in the yield of J/ψ mesons. It is found to be qualitatively similar to the trends observed at previous, lower-energy experiments. The relative yields of Z bosons as a function of centrality are also presented, although the low statistics precludes any strong conclusions. These results provide a first look at the modification of high-p_T processes in heavy-ion collisions at the highest-available beam energy.

PACS 25.75.-q – Relativistic heavy-ion collisions.

1. – Heavy-ion physics with the ATLAS detector at the LHC

Collisions of heavy ions at ultra-relativistic energies are expected to produce an evanescent hot, dense state, with temperatures exceeding several trillion kelvins, in which the relevant degrees of freedom are not hadrons, but quarks and gluons. The ATLAS detector [1], a schematic diagram of which is shown in fig. 1, is a powerful tool for studying lead-lead collisions at the LHC energy of $\sqrt{s_{NN}} = 2.76\,\text{TeV}$ in the nucleon-nucleon center-of-mass frame. The Inner Detector measures charged-particle tracks for $|\eta| < 2.5$, the longitudinally segmented calorimeter provides electromagnetic and hadronic energy measurements for $|\eta| < 4.9$ and the Muon Spectrometer identifies and measures muons for $|\eta| < 2.7$.

2. – Jet quenching

In the hot, dense medium, high-energy quarks and gluons are expected to transfer energy to the medium by multiple interactions with the ambient plasma. There is a rich theoretical literature on in-medium QCD energy loss extending back to Bjorken, who proposed to look for "jet quenching" in proton-proton collisions [2]. This work also

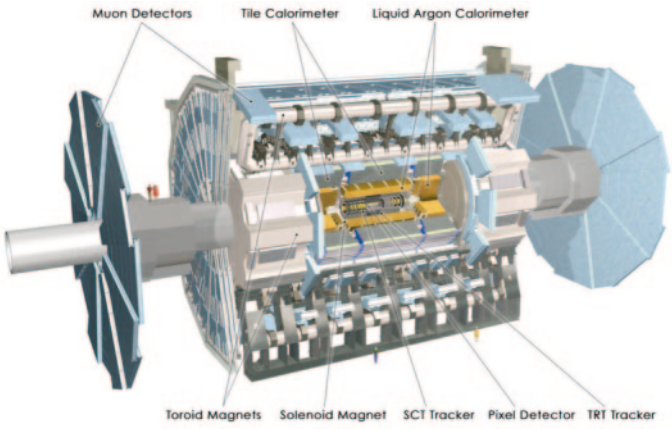

Fig. 1. – Schematic diagram of the ATLAS detector, showing the three main subsystems: the Inner Detector ($|\eta| < 2.5$), the Calorimeter ($|\eta| < 4.9$) and the Muon Spectrometer ($|\eta| < 2.7$).

suggested the observation of highly unbalanced dijets when one jet is produced at the periphery of the collision. For comprehensive reviews of recent theoretical work in this area, see refs. [3, 4].

The first LHC result on jet quenching was published by ATLAS shortly after the start of the 2010 heavy ion run [5]. To look for jet quenching, the jet energy imbalance is expressed in terms of the asymmetry A_J,

$$A_J = \frac{E_{T1} - E_{T2}}{E_{T1} + E_{T2}}, \qquad \Delta\phi > \frac{\pi}{2}, \tag{1}$$

where the first jet is required to have a transverse energy $E_{T1} > 100\,\text{GeV}$, and the second jet is the highest-transverse-energy jet in the opposite hemisphere with $E_{T2} > 25\,\text{GeV}$. Focusing on the highest-transverse-energy pair of jets in events where those jets have an azimuthal angle separation, $\Delta\phi = |\phi_1 - \phi_2| > \pi/2$ reduces contributions from multijet final states. The average contribution of the underlying event energy is subtracted when deriving the individual jet transverse energies. The event selection is chosen such that the first jet has nearly 100% reconstruction efficiency and the second jet is typically (but not always) above the distribution of background fluctuations and the intrinsic soft jets associated with the collision. Dijet events are expected to have A_J peaked near zero, albeit with large deviations arising from a variety of effects. Energy loss of one or both jets in the medium would be expected to lead to much stronger deviations in the reconstructed energy balance.

The primary event triggers were based on coincidence signals from two sets of Minimum Bias Trigger Scintillator (MBTS) detectors, positioned at $z = \pm 3.56\,\text{m}$, covering the full azimuth in the range $2.09 < |\eta| < 3.84$, as well as the Zero-Degree Calorimeters (ZDCs). These triggers have a large overlap and are close to fully efficient for the events studied here. In the offline analysis, events are required to have a time difference between the two sets of MBTS counters of $\Delta t < 3\,\text{ns}$ and a reconstructed vertex to efficiently reject beam-halo backgrounds. The primary vertex is derived from the reconstructed tracks in the Inner Detector (ID), which covers $|\eta| < 2.5$ with silicon pixel and strip detectors

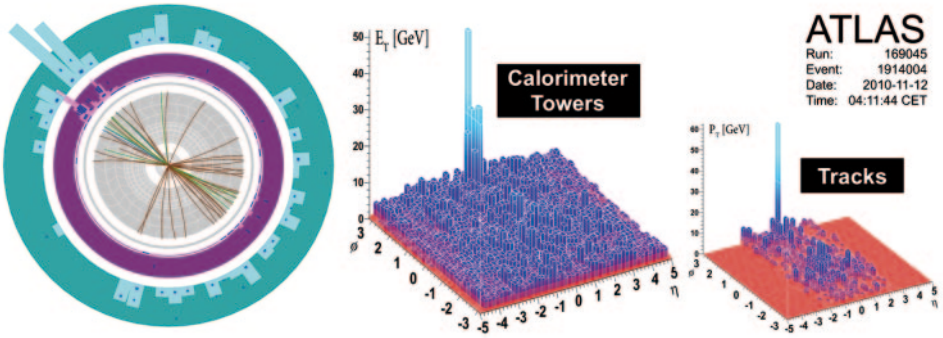

Fig. 2. – Event display of a highly asymmetric dijet event, with one jet with $E_T > 100\,\text{GeV}$ and no evident recoiling jet, and with high-energy calorimeter cell deposits distributed over a wide azimuthal region. By selecting tracks with $p_T > 2.6\,\text{GeV}$ and applying cell thresholds in the calorimeters ($E_T > 700\,\text{MeV}$ in the electromagnetic calorimeter, and $E > 1\,\text{GeV}$ in the hadronic calorimeter) the recoil can be seen dispersed widely over azimuth.

surrounded by straw tubes. These event selection criteria have been estimated to accept about 98% of the total lead-lead inelastic cross section.

Event centrality is characterized using the total transverse energy (ΣE_T) deposited in the Forward Calorimeters (FCal) covering $3.2 < |\eta| < 4.9$. Bins are defined in centrality according to fractions of the total lead-lead cross section selected by the trigger and are expressed in terms of percentiles (0–10%, 10–20%, 20–40% and 40–100%) with the 0–10% bin containing the most central events. Previous heavy ion experiments have shown a clear correlation of the ΣE_T with the geometry of the overlap region of the colliding nuclei and, correspondingly, the total event multiplicity. This is verified by the observation of a tight correlation between the transverse energy emitted near mid-rapidity and that measured at forward angles. Ultimately, the forward ΣE_T is used for this analysis to avoid any bias on the centrality measurement due to the presence of jets.

Jets have been reconstructed using the infrared-safe anti-k_t jet clustering algorithm [6] with the radius parameter $R = 0.4$. The inputs to this algorithm are towers of calorimeter cells of size $\Delta\eta \times \Delta\phi = 0.1 \times 0.1$ with the input cells weighted using energy-density–dependent factors (the so-called "H1 weights") to correct for calorimeter non-compensation and other energy losses. Jet four-momenta are constructed by the vectorial addition of cells, treating each cell as an $(E, \vec{p})$ four-vector with zero mass.

After event selection, the requirement of a leading jet with $E_T > 100\,\text{GeV}$ and $|\eta| < 2.8$ yields a sample of 1693 events. A striking feature of this sample is the appearance of events with only one high-E_T jet clearly visible in the calorimeter, and no high-E_T jet opposite to it in azimuth. Such an event is shown in fig. 2. The calorimeter E_T and the sum of charged particle p_T are shown in regions of $\Delta\eta \times \Delta\phi = 0.1 \times 0.1$. Inspection of this event shows a highly-asymmetric pair of jets with the particle and energy flow recoiling against the leading jet being widely distributed in azimuth. The lead-lead data are also compared with a sample of $17\,\text{nb}^{-1}$ of proton-proton collision data [7], which yields 6732 events.

To quantify the transverse energy balance between jets, we calculate the dijet asymmetry, A_J between the highest E_T (leading) jet and the highest E_T jet in the opposite hemisphere (second jet). This is done for each centrality bin. The second jet is required

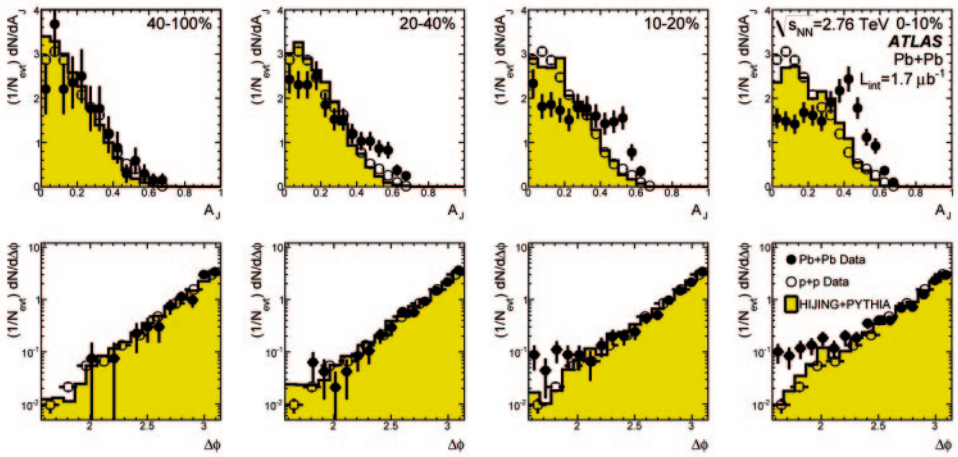

Fig. 3. – Top: Dijet asymmetry distributions for data (points) and unquenched HIJING with superimposed PYTHIA dijets (solid yellow histograms), as a function of collision centrality (left to right from peripheral to central events). Proton-proton data from $\sqrt{s} = 7\,\text{TeV}$, analyzed with the same jet selection, is shown as open circles. Bottom: Distribution of $\Delta\phi$, the azimuthal angle between the two jets, for data and HIJING+PYTHIA, also as a function of centrality.

to have $E_T > 25\,\text{GeV}$ in order to discriminate against background from the underlying event. It is found that around 5% of the jet selected events in the 40% most-central collisions have no second jet satisfying these cuts, while the more peripheral samples generally always have a dijet pair.

The dijet asymmetry and $\Delta\phi$ distributions are shown in four centrality bins in fig. 3, where they are compared with proton-proton data and with fully reconstructed simulated HIJING [8] events embedded with PYTHIA [9] dijets (the latter to illustrate the magnitude of instrumental effects). The dijet asymmetry in peripheral lead-lead events is similar to that in both proton-proton and simulated events. As the events become more central, the lead-lead data distributions show an increased rate of highly asymmetric dijet events. The asymmetry distribution broadens; the mean shifts to higher values; the peak at zero asymmetry is no longer visible; and for the most central events a small (and not very significant) peak can be seen at higher asymmetry values. It is notable that the $\Delta\phi$ distributions show that the leading and second jets are primarily back-to-back in all centrality bins, although a noticeable tail develops for the most central events at large angles relative to the recoil direction.

Numerous studies have been performed to verify that the events with large asymmetry are not produced by backgrounds or detector effects. Detector effects primarily include readout errors and local acceptance loss due to dead channels and detector cracks. All of the jet events in this sample were checked, and no events were flagged as problematic. Furthermore, the highly-asymmetric dijets were not found to populate any specific region of the calorimeter, indicating that no substantial fraction of produced energy was lost in an inefficient or uncovered region. Asymmetric jet events were found to be uncorrelated with the presence of high energy muons or missing energy (*e.g.*, from W decays). Ultimately, the asymmetry appears to be a robust result, confirmed recently by other LHC experiments (*e.g.*, ref. [10]), and turns out to be the first indication that jet quenching can be observed at the jet level, rather than just the hadron level.

3. – J/Ψ suppression and Z observation

The measurement of quarkonia production in ultra-relativistic heavy-ion collisions provides a potentially powerful tool for studying the properties of hot and dense matter created in these collisions. If deconfined matter is formed, then color screening is expected to prevent the formation of quarkonium states when the screening length becomes shorter than the quarkonium size [11]. As this length is directly related to the temperature, a measurement of a suppressed quarkonium yield may provide direct experimental sensitivity to the temperature of the medium created in high energy nuclear collisions [12]. The interpretation of J/ψ suppression in terms of color screening is generally complicated by the quantitative agreement between the overall levels of J/ψ suppression measured by the NA50 experiment at the CERN SPS [13] ($\sqrt{s_{NN}} = 17.3\,\text{GeV}$) and the PHENIX experiment at RHIC [14] ($\sqrt{s_{NN}} = 200$ GeV). Data from proton-nucleus and deuteron-gold collisions also show decreased rates of J/ψ production [15], indicating that mechanisms unrelated to color screening may also be relevant. Finally, there exist proposals for J/ψ enhancement at high energies from charm quark recombination [16]. Measurements at higher energies, with concomitantly higher temperatures and heavy quark production rates, are clearly needed to address these debates with new experimental input. The production of Z bosons, only available in heavy-ion collisions at LHC energies, can serve as a reference process for J/ψ production, since Z's are not expected to be affected by the hot, dense medium, although modifications to the nuclear parton distribution functions must be considered [17]. The first measurement of both J/ψ and Z bosons were published by ATLAS in ref. [18].

In ATLAS, muons are measured by combining independent measurements of the muon trajectories from the Inner Detector (ID) and the Muon Spectrometer (MS). The Inner Detector volume is immersed in a 2 T field and measures the trajectories of charged particles in the pseudorapidity region $|\eta| < 2.5$. A charged particle typically traverses three layers of silicon pixel detectors, eight silicon strip sensors (SCT detector) arranged in four layers of double-sided modules, and a transition radiation tracker composed of straw tubes (the latter being excluded from the present analysis). The MS surrounds the calorimeters and provides tracking for muons with $|\eta| < 2.7$ and triggering in the range $|\eta| < 2.4$. Muon momentum determination is based on three stations of precision drift chambers that measure the trajectory of each muon in a toroidal magnetic field produced by three air-core toroids. In order to reach the MS, muons have to cross the electromagnetic and hadronic calorimeters, losing typically 3 to 5 GeV of energy, depending on the muon pseudorapidity. The calorimeters efficiently absorb the copious charged and neutral hadrons produced in lead-lead collisions, keeping the muon spectrometer occupancy low.

The same conventions for collision centrality are used as described previously. The centrality dependence of the muon detection efficiency is parameterized as a function of the total number of hits per unit of pseudorapidity detected in the first pixel layer. This is strongly correlated with $\Sigma E_{\mathrm{T}}^{\mathrm{FCal}}$, but gives a more direct measure of the ID occupancy. The full data sample is divided into four bins of collision centrality, 40–80%, 20–40%, 10–20%, and 0–10%. The most peripheral 20% of collisions are excluded from this analysis due to larger systematic uncertainties in estimating the number of binary nucleon-nucleon collisions in these events, which are derived using a Monte Carlo Glauber calculation [19, 20].

The $J/\psi \to \mu^+\mu^-$ reconstruction efficiency is obtained from the MC samples as a function of centrality. The inefficiency gradually increases from peripheral to central collisions, due primarily to an occupancy-induced inefficiency in the ID tracking.

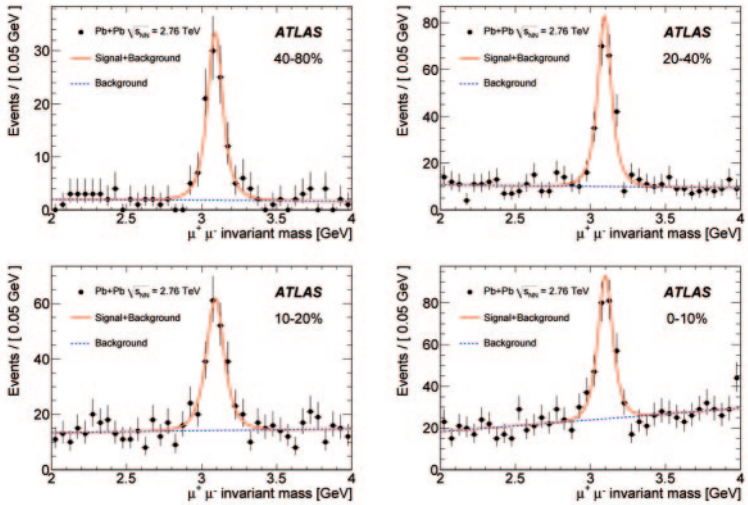

Fig. 4. – Oppositely charged dimuon invariant-mass spectra in the four considered centrality bins from most peripheral (40–80%) to most central (0–10%). The J/ψ yields in each centrality bin are obtained using a sideband technique. The fits shown here are used only as a cross-check.

The oppositely charged dimuon invariant mass spectra in the J/ψ region after the selection are shown in fig. 4. The number of $J/\psi \to \mu^+\mu^-$ decays is then found by a sideband technique, with the signal mass window from 2.95–3.25 GeV. and the background sidebands defined in 2.4–2.8 GeV and 3.4–3.8 GeV. To determine the uncertainties related to the signal extraction, an alternative method based on a maximum-likelihood fit with the mass resolution left as a free parameter is used as a cross check. With the chosen transverse momentum cuts on the decay muons, 80% of the reconstructed J/ψ have $p_T > 6.5$ GeV.

The measured J/ψ yields at different centralities are corrected by the reconstruction efficiency ϵ_c for $J/\psi \to \mu^+\mu^-$, derived from MC and parameterized in each centrality bin, and the width of the centrality bin, W_c, which represents a well-defined fraction of the minimum bias events. The corrected yield of J/ψ mesons is given by

$$N_c^{\mathrm{corr}}(J/\psi \to \mu^+\mu^-) = \frac{N^{\mathrm{meas}}(J/\psi \to \mu^+\mu^-)_c}{\epsilon(J/\psi)_c \cdot W_c}\,. \tag{2}$$

The "relative yield" is defined by normalizing to the yield found in the most peripheral 40–80% centrality bin: $R_c = N_c^{\mathrm{corr}}/N_{40-80\%}^{\mathrm{corr}}$. Note that the uncertainties in the 40–80% bin are not propagated into this ratio for the more central bins. Finally, the "normalized yield" is defined by scaling the relative yield by the ratio R_{coll} which is the mean number of binary collisions $N_{\mathrm{coll},c}$ in each centrality bin divided by that for the most peripheral (40–80%) bin: $R_{cp} = R_c/R_{\mathrm{coll}}$. The total systematic uncertainties on the ratios R_{coll} are evaluated by combining the variations of the various parameters going into the Glauber calculation (radius, skin depth, nucleon-nucleon cross section, and the fraction of the minimum-bias cross section sampled by the trigger and event selection) in quadrature.

The relative J/ψ yields after normalization and efficiency corrections as in equation (2), R_c, are compared to the expected R_{coll} values in the left panel of fig. 5. The yield

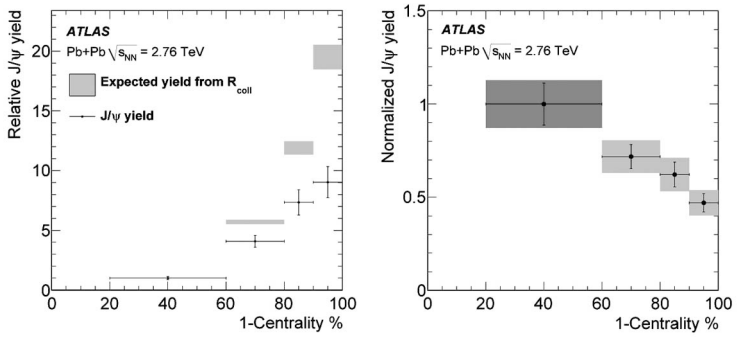

Fig. 5. – Left: Relative J/ψ yield as a function of centrality normalized to the most peripheral bin (black dots with errors). The expected relative yields from the (normalized) number of binary collisions ($R_{\rm coll}$) are also shown (boxes, reflecting 1σ systematic uncertainties). Right: Value of R_{cp}, as described in the text, as a function of centrality. The statistical errors are shown as vertical bars while the grey boxes also include the combined systematic errors. The uncertainties for the most peripheral bin are not propagated into the more central ones.

errors are computed by adding the statistical and systematic uncertainties in quadrature. A clear difference is observed as a function of centrality between the measured relative J/ψ yield and the prediction based on $R_{\rm coll}$, indicating a deviation from the simplest expectation based on QCD factorization. The ratio of these two values, R_{cp}, is shown as a function of centrality in the right panel of fig. 5. The data points are not consistent with a fit to a constant value giving a $P(\chi^2, N_{\rm DOF})$ value of 0.11% with three degrees of freedom. Instead, a significant decrease of R_{cp} as a function of centrality is observed.

Z candidates are selected by requiring a pair of oppositely charged muons with $p_{\rm T} > 20\,{\rm GeV}$ and $|\eta| < 2.5$ [21]. We apply an additional cosmic ray rejection cut on the sum of the pseudorapidities of the two muons, $|\eta_1 + \eta_2| > 0.01$. The invariant mass distribution of the selected pairs is shown in the left panel of fig. 6. With this selection, 38 Z candidates

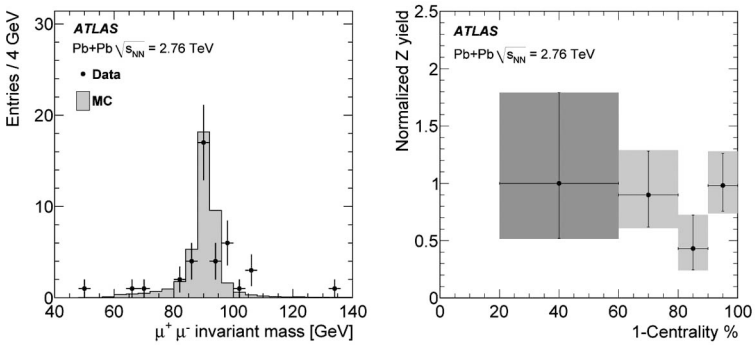

Fig. 6. – The dimuon invariant mass (left) after the selection described in the text. The value of R_{cp} (right) computed with the 38 selected Z candidates. The statistical errors are shown as vertical bars while the grey boxes also include the combined systematic errors. The darker box indicates that the 40–80% bin is used to set the scale for all bins, but the uncertainties in this bin are not propagated into the more central ones.

are retained in the signal mass window of 66 to 116 GeV. The background after this selection is expected to be below 2%, and is not corrected for in the result.

The R_{cp} variable for the Z candidates is computed in the same way as for the J/ψ sample. The same systematic uncertainties as for the J/ψ results have been applied to the Z relative yield measurements. Several cross-checks have been performed to support this approach. In addition to the tracks reconstructed with the combined ID and MS information, tracks reconstructed by the MS alone have been checked, and only one additional candidate was found. In the Z mass window, no candidate was found using same-charge muon pairs. Cosmic rays were rejected by studies of the transverse impact parameter distributions.

The measured Z yields are displayed in the right panel of fig. 6, normalized to the yield in the most peripheral bin and to the number of binary collisions (R_{cp}). The Z yields appear to be compatible with a linear scaling with the number of binary collisions, altohugh the low statistics preclude drawing any strong conclusions.

4. – Conclusions and outlook

The first results from the ATLAS detector using data from the LHC heavy-ion run are presented. The first published observations of strong dijet asymmetry clearly confirm previous reports of jet quenching in heavy ion collisions using high-momentum hadrons, but show that the suppression can be seen at the jet level. A systematic suppression of high-momentum J/ψ mesons near mid-rapidity is also observed, with a centrality dependence similar to that seen for inclusive J/ψ at lower energies. The first observation of Z bosons show no strong deviations from the expected scaling with the number of binary collisions, but the low statistics preclude strong conclusions.

* * *

The author would like to thank the La Thuile organizers for the invitation, the ATLAS Collaboration for providing an excellent environment to do heavy-ion physics, and the LHC team for superlative performance of the machine during the first lead-lead run.

REFERENCES

[1] Aad G. *et al.* (ATLAS Collaboration), *JINST*, **3** (2008) S08003.
[2] Bjorken J. D., FERMILAB-PUB-82-059-THY (1982).
[3] Wiedemann U. A., arXiv:0908.2306 [hep-ph].
[4] Majumder A. and Van Leeuwen M., arXiv:1002.2206 [hep-ph].
[5] Aad G. *et al.* (ATLAS Collaboration), *Phys. Rev. Lett.*, **105** (2010) 252303.
[6] Cacciari M., Salam G. P. and Soyez G., *JHEP*, **0804** (2008) 63.
[7] Aad G. *et al.* (ATLAS Collaboration), *Eur. Phys. J. C*, **71** (2011) 1512.
[8] Wang X.-N. and Gyulassy M., *Phys. Rev. D*, **44** (1991) 3501.
[9] Sjostrand T., Mrenna S. and Skands P. Z., *JHEP*, **0605** (2006) 26.
[10] Chatrchyan S. *et al.* (CMS Collaboration), arXiv:1102.1957 [nucl-ex].
[11] Matsui T. and Satz H., *Phys. Lett. B*, **178** (1986) 416.
[12] Mocsy A. and Petreczky P., *Phys. Rev. Lett.*, **99** (2007) 211602.
[13] Alessandro B. *et al.* (NA50 Collaboration), *Eur. Phys. J. C*, **39** (2005) 335-345.
[14] Adare A. *et al.* (PHENIX Collaboration), *Phys. Rev. Lett.*, **98** (2007) 232301.

[15] Badier J. *et al.* (NA3 Collaboration), *Z. Phys. C*, **20** (1983) 101; Abreu M. C. *et al.* (NA38 Collaboration), *Phys. Lett. B*, **444** (1998) 516; Leitch M. J. *et al.* (FNAL E866 Collaboration), *Phys. Rev. Lett.*, **84** (2000) 3256; Alessandro B. *et al.* (NA50 Collaboration), *Eur. Phys. J. C*, **33** (2004) 31; Alessandro B. *et al.* (NA50 Collaboration), *Eur. Phys. J. C*, **48** (2006) 329; Abt I. *et al.* (HERA-B Collaboration), *Eur. Phys. J. C*, **60** (2009) 525; Adare A. *et al.* (PHENIX Collaboration), *Phys. Rev. Lett.* **107** (2011) 142301.
[16] Thews R. L. and Mangano M. L., *Phys. Rev. C*, **73** (2006) 014904.
[17] Vogt R., *Phys. Rev. C*, **64** (2001) 044901.
[18] Aad G. *et al.* (The ATLAS Collaboration), *Phys. Lett. B*, **697** (2011) 294.
[19] Alver B., Baker M., Loizides C. *et al.*, arXiv:0805.4411 [nucl-ex].
[20] Miller M. L., Reygers K., Sanders S. J. *et al.*, *Annu. Rev. Nucl. Part. Sci.*, **57** (2007) 205.
[21] Aad G. *et al.* (ATLAS Collaboration), *JHEP*, **1012** (2010) 60.